Estimating atmospheric profiles with WRF model and comparative analysis of Planetary Boundary Layer schemes

Lucas Ribeiro Diaz[1], Daniel Caetano Santos[2], Pâmela Suélen Käfer[1], María Luján Iglesias[1], Nájila Souza da Rocha[1], Savannah Tâmara Lemos da Costa[1], Eduardo Andre Kaiser[1], Silvia Beatriz Alves Rolim[1], [1]Universidade Federal do Rio Grande do Sul (UFRGS) - State Research Center for Remote Sensing and Meteorology (CEPSRM), [2]Universidade Federal de Santa Maria (UFSM) - Department of Physics. [Contact: lucas.diaz@ufrgs.br]

Abstract

Atmospheric profiles are pivotal for satellite data calibration. In this work, we assess the use of the Weather Research and Forecasting (WRF) model to refine NCEP Climate Forecast System Version 2 (CFSv2) reanalysis atmospheric profiles. In addition, a sensitivity analysis was conducted to Yonsei University (YSU) and Mellor–Yamada–Janjic (MYJ) Planetary Boundary Layer (PBL) parameterization schemes. WRF simulations were performed using two nested grids with horizontal resolutions of 12 and 3 km. Estimated profiles were evaluated against radiosonde observations at Southern Brazil. WRF satisfactorily simulates vertical profiles of water vapor mixing ratio (q) and potential temperature (θ). The comparison yielded high correlation coefficients (mostly higher than 0.9), low average biases (moist and cold), and overall RMSE of 0.84 g/Kg and 2.30 K for q and θ, respectively. There is no significant statistical difference in the profiles on increasing the horizontal resolution. The overall results did not indicate any preferred PBL scheme that outperforms in all cases. The WRF model and even data directly from NCEP CFSv2 reanalysis are useful to represent the vertical structure of the atmosphere.

Introduction

The vertical distribution of atmospheric parameters is essential to modeling weather and climate on regional and global scales (Sobrino et al., 2015). Atmospheric temperature and water vapor play a crucial role in the thermodynamic state of the atmosphere (De Rosa et al., 2020; Jiang et al., 2019; Sherwood et al., 2010; Thorne et al., 2005). An important application of vertical profiles is in the atmospheric correction of thermal infrared (TIR) remote sensing data to retrieve land surface temperature (LST) information (Barsi et al., 2003; Coll et al., 2012; Jiménez-Muñoz et al., 2010; Meng and Cheng, 2018; Rosas et al., 2017). LST is a key parameter indicating the relationship between land-atmosphere since it is connected to the Earth's surface energy balance (Tardy et al., 2016).

A radiosonde profile can characterize the atmospheric structure at a specific location with high precision. However, it is only available at limited sites (usually in urban areas) and times (typically 00:00 and 12:00 UTC) (Alghamdi, 2020; De Rosa et al., 2020; Filioglou et al., 2017). So radiosonde-recorded data is particularly regarded as the truth value in validation studies and calibration of satellite data (Divakarla et al., 2006; Meng and Cheng, 2018; Rao et al., 2020).

Reanalysis data from global numerical models are a practical alternative to the radiosondes spatiotemporal limitations (Rosas et al., 2017). In these datasets, numerical weather prediction outputs, data assimilation techniques, and observations from several data sources are combined to characterize the state of the atmosphere at different spatiotemporal scales. The resulting data set is global gridded with an extended homogeneous time series (Alghamdi, 2020; Mooney et al., 2011). Even though global reanalysis data are widely applied in scientific research, their accuracy is generally lower for regions with poor permanent observatories coverage, such as many Southern Hemisphere regions and the oceans (Chen and Liu, 2016; Chen et al., 2014). Moreover, reanalysis data may have the accuracy of meteorological phenomena on a sub-grid or variable time scale affected since they are spaced at grid points with time intervals of typically 6 h (Tonooka, 2001).

Therefore, coarse global-scale data may not be suitable for local use. Modern Numerical Weather Prediction (NWP) models enjoy great computing performance and parameterization of physical processes to improve the reanalysis data accuracy (Evans et al., 2012; Prasad et al., 2020). Mesoscale atmospheric models are used in local areas with global models data as the boundary and initial conditions (Hassanli and Rahimzadegan, 2019; Wee et al., 2012). The Weather Research and Forecasting (WRF) model (Skamarock et al., 2019) is a state-of-the-art atmospheric modeling system designed for both meteorological research and NWP (Onwukwe and Jackson, 2020; Powers et al., 2017; Prasad et al., 2020). Non-hydrostatic, community-based, free, and open-source, the WRF model provides specialized resources for a variety of applications in terrestrial systems (Powers et al., 2017; Skamarock et al., 2019). It is among the most frequently used mesoscale models for estimating high-resolution meteorological data (Hassanli and Rahimzadegan, 2019; Knievel et al., 2007; Powers et al., 2017).

Nevertheless, many atmospheric physical processes cannot be completely resolved by the numerical model and must be parameterized (García-Díez et al., 2013; Stensrud, 2007; Xie et al., 2012). Among them, the Planetary Boundary Layer (PBL) parameterization is crucial to the simulation of meteorological properties (Hu et al., 2010; Jia and Zhang, 2020; Xie et al., 2012). PBL is the portion of the troposphere closest to the ground level, characterized by friction and turbulent mixing (Stull, 2017). Vertical profiles of temperature and water vapor can exhibit variances among the PBL schemes across the PBL depth and subsequently the entire atmospheric column and the whole model domain (Chaouch et al., 2017; Cuchiara et al., 2014; Hariprasad et al., 2014; Hu et al., 2010; Xie et al., 2012). Additionally, PBL is where the highest concentrations of water vapor in the atmosphere are located, which is the principal factor for atmospheric effects in TIR optical satellite images (Jiménez-Muñoz et al., 2010; Sobrino et al., 1991). The WRF model has a wide range of physical parameterizations options, and so it is with boundary layer schemes. Several sensitivity studies to PBL schemes have been carried out (Chaouch et al., 2017; Cuchiara et al., 2014; García-Díez et al., 2013; Hariprasad et al., 2014; Hu et al., 2010; Onwukwe and Jackson, 2020; Ruiz et al., 2010). But there is a general lack of sensitivity studies on the effect of different PBL parameterization schemes over South America (Jia and Zhang, 2020).

This study aims to assess the reasonableness of the WRF as a tool to downscaling reanalyze atmospheric profiles to their use in future assessments for atmospheric correction of TIR remote sensing images. Thus, we expect to generate high-resolution vertical profiles as an alternative to the need for a radiosonde. We conducted WRF simulations using as initial and boundary conditions the National Centers for Environmental Prediction (NCEP) Climate Forecast System Version 2 (CFSv2) (Saha et al., 2014) reanalysis data. In addition, a sensitivity analysis was carried out with the two widely used PBL schemes: Yonsei University (YSU) and Mellor–Yamada–Janjic (MYJ). Since each PBL scheme is tied to a particular surface-layer scheme, Revised MM5 and Eta Similarity schemes were used, respectively. The model simulations were evaluated with available radiosonde observations at a station in Southern Brazil.

Method

Numerical simulations were performed using the WRF Model version 4.1.2 with the Advanced Research WRF (ARW) dynamical solver (Skamarock et al., 2019; Wang et al., 2019). The models' domain was configured with two nested grids with horizontal resolutions of 12 km (G12) and 3 km (G03) (4:1 parent grid ratio), in one-way mode, and 33 sigma vertical levels with 50 hPa top pressure value. The nested grids were centered at the radiosonde station of the Porto Alegre International Airport (SBPA), Rio Grande do Sul State, Brazil. The station is located at 30.00º S and 51.18º W, with a 3.0 m elevation above mean sea level. In SBPA station, radiosondes are launched twice a day, at 00:00 and 12:00 UTC. These radiosonde observations will serve as ground truth for validation and evaluation of the simulations. Figure 1 shows the model grids and also an asterisk that indicates where the simulation results were extracted, it refers to the grid point closest to the SBPA station.

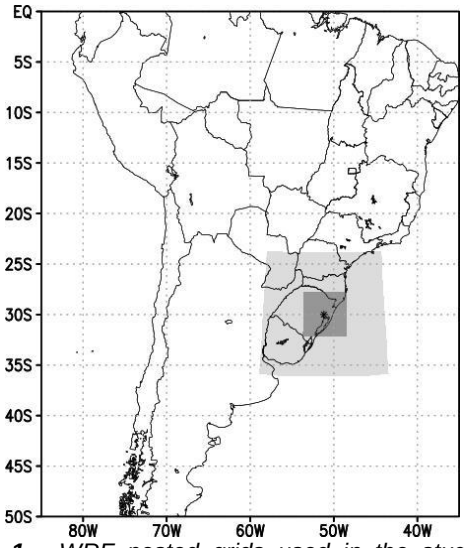

Figure 1 - *WRF nested grids used in the study, with horizontal resolutions of 12 km (light gray) and 3 km (dark gray). The asterisk indicates the point where the results were extracted.*

The WRF model set ups are resumed in Table 1. A sensitivity experiment was conducted by changing the PBL and the surface-layer parameterization schemes. The YSU PBL scheme (Hong et al., 2006) was used tied to the Revised MM5 surface-layer scheme (Jiménez et al., 2012), and MYJ (Janjić, 1994) combined with Eta Similarity (Janjić, 2002, 1996, 1994; Monin and Obukhov, 1954). Similar choices of parameterization schemes were used in Santos and Nascimento (2016).

Table 1 - *Overview of WRF model configuration.*

WRF Model Configuration	
Version	4.1.2
Dynamical solver	ARW
Boundary conditions	NCEP CFSv2
Map projection	Lambert
Grid size	Domain 1: (119 x 116) x 33
	Domain 2: (169 x 165) x 33
Horizontal resolution	Domain 1: 12 km
	Domain 2: 3 km
Nesting	One-way
Time step	72s
Static geographical data	USGS
Cloud Microphysics	Purdue Lin
PBL	1) YSU
	2) MYJ
Cumulus	BMJ (Domain 1 only)

Shortwave Radiation	Dudhia
Longwave Radiation	RRTM
LSM	Unified NOAH
Surface-layer	1) Revised MM5
	2) Eta Similarity

We are particularly interested in the performance of high-resolution vertical profiles for atmospheric correction of TIR remote sensing data purposes. So our study is developed for dates coinciding with the Landsat 8 passage over the SBPA under clear-sky conditions. Table 2 shows the dates used in this work, i.e., the 27 days when clear-sky Landsat 8 images were available from 2013 to 2019. In addition, we use the 12:00 UTC radiosonde profiles as reference, since this is the closest time to the Landsat 8 crossing time over the study area (~13 UTC).

The study consisted of 54 runs of 24-h duration for the 27 selected dates in Table 2: a simulation with YSU and another with MJY PBL option for each of the days. The resulting profiles were extracted at 12:00 UTC, to match with the in situ radiosonde observations. So the first 12 h of the simulation was considered for spin up time.

Table 2 - *Dates used to perform the study.*

Year	Day and Month (Case Day)		
2013	18 Nov (1)	04 Dec (2)	
2014	06 Feb (3)	20 Oct (4)	07 Dec (5)
2015	24 Jan (6)	25 Feb (7)	08 Nov (8)
2016	15 Mar (9)	22 Aug (10)	12 Dec (11)
2017	03 Apr (12)	22 Jun (13)	24 Jul (14)
	25 Aug (15)	13 Nov (16)	15 Dec (17)
2018	17 Feb (18)	22 Apr (19)	09 Jun (20)
	28 Aug (21)	29 Sep (22)	16 Nov (23)
2019	24 Mar (24)	09 Apr (25)	15 Aug (26)
	19 Nov (27)		

To evaluate the accuracy of the model simulations and the impact of the PBL schemes, we take into account vertical profiles of water vapor mixing ratio (q) and potential temperature (θ). A point validation technique was used (Onwukwe and Jackson, 2020). Atmospheric profiles for model grid point corresponding to the ground location of the SBPA station (Figure 1) were retrieved, at 12 UTC. Namely, the WRF resulting profiles of q and θ for G12 and G03, and with both YSU and MYJ schemes were intercompared against SBPA observational profiles. Besides that, profiles retrieved directly from the CFSv2 product were included in the comparative analysis to assess the performance of the WRF in downscaling reanalysis profiles.

Vertical interpolation for a comparison of model output to observations is imperative since the height and pressure of model (sigma) levels can vary both spatially and temporally in the model domain (Cogan, 2017). Therefore, the WRF output data were interpolated from the model to the radiosondes vertical levels. The interpolation was carried out through a weighted linear one (Santos and Nascimento, 2016). The statistical criteria used in this paper are Pearson's correlation coefficient (R), bias (mean error), Mean Absolute Error (MAE), and Root Mean Square Error (RMSE).

Results and discussion

To evaluate the performances of the different atmospheric profiles, they were extracted from the grid point closest to the SBPA station at 12 UTC. Figure 2 shows an example of the vertical distribution of q and θ for the case day 6. It indicates a good agreement of CFSv2 reanalysis and all WRF settings profiles with the radiosonde observations.

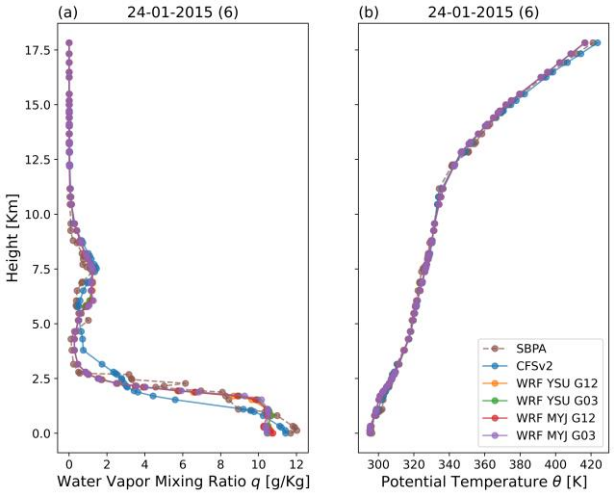

Figure 2 - *Vertical profiles of (a) water vapor mixing ratio and (b) potential temperature for the case 6 (24-01-2015).*

Figure 3 illustrates the statistical comparison of the studied profiles throughout each case day for q and θ. While Table 3 presents the average metrics of profiles comparison for all evaluated days. The CFSv2 and all WRF profiles showed the same high correlation coefficient values for the vertical distribution of both q (0.96) and θ (0.99). All q profiles showed a mean tendency to overestimate the observations (positive bias), with CFSv2 showing the highest bias (0.10 g/Kg). The q bias of G12 grids was slightly higher than one of the G03. On the other hand, the WRF configurations tend to underestimate the θ vertical distribution, while CFSv2 reanalysis tends to overestimate it (see Figure 3a). The CFSv2 θ bias was the largest (0.50 K). There was no significant difference between the overall biases of WRF YSU and MYJ.

Moreover, the WRF MYJ had the highest MAE for q (0.44 g/Kg), with a small variation in comparison to WRF YSU and CFSv2 (0.43 g/Kg). The θ MAE of the WRF profiles was larger: 1.60 K against 1.57 K of the CFSv2. In terms

of RMSE, all the WRF sets showed the same value which was slightly worse than for the CFSv2 (see Table 3).

Table 3 - *Statistical comparison of all q and θ model profiles against SBPA radiosonde observations.*

	CFSv2	WRF YSU G12	WRF YSU G03	WRF MYJ G12	WRF MYJ G03
R *q*	0.96	0.96	0.96	0.96	0.96
bias *q* [g/Kg]	0.10	0.04	0.03	0.04	0.03
MAE *q* [g/Kg]	0.43	0.43	0.43	0.44	0.44
RMSE *q* *[g/Kg]*	0.82	0.84	0.84	0.84	0.84
R *θ*	0.99	0.99	0.99	0.99	0.99
bias *θ* [K]	0.50	-0.20	-0.20	-0.20	-0.21
MAE *θ* [K]	1.57	1.61	1.61	1.61	1.61
RMSE *θ* [K]	2.22	2.30	2.30	2.30	2.30

The RMSE and MAE overall values of the WRF simulations were a bit higher than those from NCEP CFSv2. However, taking into account each individual case day, the WRF model (including all the settings analyzed) overcomes the CFSv2 reanalysis in more days than the opposite for water vapor mixing ratio profiles. We have found WRF settings with the best RMSE in 14 of the 27 case days and with the best MAE in 19. For potential temperature, the WRF settings overcome the CFSv2 in 13 of the 27 case days. Case day 10 was found as the one with the largest discrepancy with observations regarding the vertical evolution of *θ* (RMSEs around 4.6 K). While in case day 17,e.g., the WRF model notably improved the high *θ* errors from the NCEP CFSv2 reanalysis (Figures 3e and 3f).

No significant statistical differences are shown between the WRF grids G12 and G03, for both parameterization schemes used. In some cases, a finer grid even increased the errors. Findings like this have already been mentioned in other papers (Diaz et al., 2020; Hassanli and Rahimzadegan, 2019; Lin et al., 2018; Mohan and Sati, 2016; Pérez-Jordán et al., 2015). These results suggest that computation costs can be saved by using a coarse horizontal resolution grid, mean-while efficiently simulate the vertical profile. Nevertheless, in at least 12 of the 27 case days, we have found an improvement in statistical metrics when the model went from 12 km to 3 km horizontal resolution. Hence, such fine grid spacing is recommended for high-resolution operational needs (Pérez-Jordán et al., 2015).

No particular PBL parameterization outperformed in all cases. Additionally, large differences between the schemes were not observed in the vertical distribution of the meteorological variables. Scholars have already reported this (Chaouch et al., 2017; Cuchiara et al., 2014; Hariprasad et al., 2014; Kioutsioukis et al., 2016; Moya-Álvarez et al., 2020; Tyagi et al., 2018). Our findings corroborate with the conclusions of García-Díez et al. (2013). The authors outlined that the performance of WRF model different settings frequently depends on the different atmospheric conditions that prevail on the different seasons and times of the day.

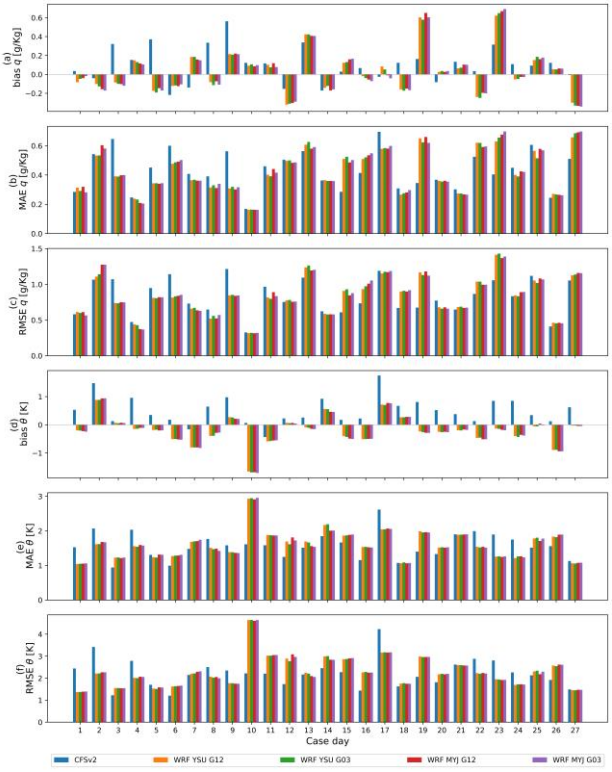

Figure 3 - *Statistical metrics over the case days: bias, MAE, and RMSE for q (a-c) and θ (d-f).*

Conclusions

Analyzing downscaled meteorological data is important to diagnose model errors that can propagate to the end application, such as the atmospheric correction of optical satellite images. In this paper, we assessed the use of WRF model version 4.1.2 to downscaling NCEP CFSv2 reanalysis vertical profiles. A sensitivity analysis was conducted with the nonlocal YSU and the local MYJ PBL schemes. Validation was performed using radiosonde observations at a station in Southern Brazil. The WRF model simulated well the vertical profiles of water vapor mixing ratio and potential temperature.

The WRF resulting profiles yielded high correlation coefficients, very small biases, and relatively low values of RMSE and MAE. However, there is no significant difference in statistical overall results of profiles WRF varying the horizontal grid resolution from 12 to 3 km, and also with those retrieved directly from NCEP CFSv2 reanalysis. These results indicate that increasing the horizontal resolution did not improve significantly the quality of the simulated atmospheric profile. Therefore,

our findings suggest that there is no special need to increase the spatial resolution for many applications (e.g., those related to average site atmosphere characterization). In such cases, it adds computational cost without expressive improvement of the simulated profiles. We recommend the use of grid spacing finer than 3 km for specific high-resolution local usages.

The sensitivity analysis of the vertical profile simulation to YSU and MYJ PBL parameterization revealed that neither particular scheme outperforms in all case days. These results emphasized that the optimal parameterization scheme set varies with local, variable, season, and meteorological conditions.

In conclusion, the WRF model is a useful tool in the simulation of water vapor and temperature atmospheric profiles. The application of both WRF and NCEP CFSv2 profiles in the atmospheric correction of remote sensing data is promising. With this in mind, further studies are underway.

Acknowledgments

This study was financed in part by the Coordenação de Aperfeiçoamento de Pessoal de Nível Superior – Brazil (CAPES), finance code 001.

References

ALGHAMDI, A.S. 2020. Evaluation of four reanalysis datasets against radiosonde over Southwest Asia. *Atmosphere*. 11(4).

BARSI, J.A.; BARKER, J.L.; SCHOTT, J.R. 2003. An Atmospheric Correction Parameter Calculator for a single thermal band earth-sensing instrument. *In*: IGARSS 2003. 2003 IEEE International Geoscience and Remote Sensing Symposium. Proceedings (IEEE Cat. No.03CH37477). IEEE, pp. 3014–3016.

CHAOUCH, N.; TEMIMI, M.; WESTON, M.; GHEDIRA, H. 2017. Sensitivity of the meteorological model WRF-ARW to planetary boundary layer schemes during fog conditions in a coastal arid region. *Atmos. Res*. 187, 106–127.

CHEN, B.; LIU, Z. 2016. Global water vapor variability and trend from the latest 36 year (1979 to 2014) data of ECMWF and NCEP reanalyses, radiosonde, GPS, and microwave satellite. *J. Geophys. Res. Atmos*. 121(19), 11,442-11,462.

CHEN, G.; IWASAKI, T.; QIN, H.; SHA, W. 2014. Evaluation of the warm-season diurnal variability over East Asia in recent reanalyses JRA-55, ERA-Interim, NCEP CFSR, and NASA MERRA. *J. Clim.* 27(14), 5517–5537.

COGAN, J. 2017. Evaluation of model-generated vertical profiles of meteorological variables: method and initial results. *Meteorol. Appl*. 24(2), 219–229.

COLL, C.; CASELLES, V.; VALOR, E.; NICLÒS, R. 2012. Comparison between different sources of atmospheric profiles for land surface temperature retrieval from single channel thermal infrared data. *Remote Sens. Environ*. 117, 199–210.

CUCHIARA, G.C.; LI, X.; CARVALHO, J.; RAPPENGLÜCK, B. 2014. Intercomparison of planetary boundary layer parameterization and its impacts on surface ozone concentration in the WRF/Chem model for a case study in houston/texas. *Atmos. Environ*. 96, 175–185.

DE ROSA, B.; DI GIROLAMO, P.; SUMMA, D. 2020. Temperature and water vapour measurements in the framework of the Network for the Detection of Atmospheric Composition Change (NDACC). *Atmos. Meas. Tech*. 13(2), 405–427.

DIAZ, L.R.; ROLIM, S.B.A.; SANTOS, D.C.; KÄFER, P.S.; ROCHA, N.S. da; ALVES, R. de C.M. 2020. Using the WRF Model to Refine NCEP CFSv2 Reanalysis Atmospheric Profile: A Southern Brazil Test Case. *Brazilian J. Geophys*. 38(2).

DIVAKARLA, M.G.; BARNET, C.D.; GOLDBERG, M.D.; MCMILLIN, L.M.; MADDY, E.; WOLF, W.; … LIU, X. 2006. Validation of Atmospheric Infrared Sounder temperature and water vapor retrievals with matched radiosonde measurements and forecasts. *J. Geophys. Res. Atmos*. 111(9), 1–20.

EVANS, J.P.; EKSTRÖM, M.; JI, F. 2012. Evaluating the performance of a WRF physics ensemble over South-East Australia. *Clim. Dyn*. 39(6), 1241–1258.

FILIOGLOU, M.; NIKANDROVA, A.; NIEMELÄ, S.; BAARS, H.; MIELONEN, T.; LESKINEN, A.; … KOMPPULA, M. 2017. Profiling water vapor mixing ratios in Finland by means of a Raman lidar, a satellite and a model. *Atmos. Meas. Tech*. 10(11), 4303–4316.

GARCÍA-DÍEZ, M.; FERNÁNDEZ, J.; FITA, L.; YAGÜE, C. 2013. Seasonal dependence of WRF model biases and sensitivity to PBL schemes over Europe. *Q. J. R. Meteorol. Soc*. 139(617), 501–514.

HARIPRASAD, K.B.R.R.; SRINIVAS, C. V.; SINGH, A.B.; RAO, S.V.B.; BASKARAN, R.; VENKATRAMAN, B. 2014. Numerical simulation and intercomparison of boundary layer structure with different PBL schemes in WRF using experimental observations at a tropical site. *Atmos. Res*. 145–146, 27–44.

HASSANLI, H.; RAHIMZADEGAN, M. 2019. Investigating extracted total precipitable water vapor from Weather Research and Forecasting (WRF) model and MODIS measurements. *J. Atmos. Solar-Terrestrial Phys*. 193, 105060.

HONG, S.-Y.; NOH, Y.; DUDHIA, J. 2006. A New Vertical Diffusion Package with an Explicit Treatment of Entrainment Processes. *Mon. Weather Rev*. 134(9), 2318–2341.

HU, X.-M.; NIELSEN-GAMMON, J.W.; ZHANG, F. 2010. Evaluation of Three Planetary Boundary Layer Schemes in the WRF Model. *J. Appl. Meteorol. Climatol*. 49(9), 1831–1844.

JANJIĆ, Z.I. 2002. Nonsingular Implementation of the Mellor-Yamada Level 2.5 Scheme in the NCEP Meso model. *NCEP Office Note* (Vol. 437).

JANJIĆ, Z.I. 1996. The surface layer in the NCEP ETA model. *In*: Eleventh Conference on Numerical Weather Prediction. Amer. Meteor. Soc., Norfolk, VA, pp. 354–355.

JANJIĆ, Z.I. 1994. The Step-Mountain Eta Coordinate Model: Further Developments of the Convection, Viscous Sublayer, and Turbulence Closure Schemes. *Mon. Weather Rev*. 122(5), 927–945.

JIA, W.; ZHANG, X. 2020. The role of the planetary boundary layer parameterization schemes on the meteorological and aerosol pollution simulations: A review. *Atmos. Res*. 239, 104890.

JIANG, J.; ZHOU, T.; ZHANG, W. 2019. Evaluation of Satellite and Reanalysis Precipitable Water Vapor Data Sets Against Radiosonde Observations in Central Asia. *Earth Sp. Sci*. 6(7), 1129–1148.

JIMÉNEZ-MUÑOZ, J.C.; SOBRINO, J.A.; MATTAR, C.; FRANCH, B. 2010. Atmospheric correction of optical imagery from MODIS and Reanalysis atmospheric products. *Remote Sens. Environ*. 114(10), 2195–2210.

JIMÉNEZ, P.A.; DUDHIA, J.; GONZÁLEZ-ROUCO, J.F.; NAVARRO, J.; MONTÁVEZ, J.P.; GARCÍA-BUSTAMANTE, E. 2012. A Revised Scheme for the WRF Surface Layer Formulation. *Mon. Weather Rev*. 140(3), 898–918.

KIOUTSIOUKIS, I.; DE MEIJ, A.; JAKOBS, H.; KATRAGKOU, E.; VINUESA, J.; KAZANTZIDIS, A. 2016. High resolution WRF ensemble forecasting for irrigation: Multi-variable evaluation. *Atmos. Res*. 167, 156–174.

KNIEVEL, J.C.; BRYAN G.H.; HACKER, J.P. 2007. Explicit numerical diffusion in the WRF model. *Mon. Weather Rev*. 135(11), 3808–3824.

LIN, C.; CHEN, D.; YANG, K.; OU, T. 2018. Impact of model resolution on simulating the water vapor transport through the central Himalayas: implication for models' wet bias over the Tibetan Plateau. *Clim. Dyn.* 51(9), 3195–3207.

MENG, X.; CHENG, J. 2018. Evaluating Eight Global Reanalysis Products for Atmospheric Correction of Thermal Infrared Sensor—Application to Landsat 8 TIRS10 Data. *Remote Sens*. 10(3), 474.

MOHAN, M.; SATI, A.P. 2016. WRF model performance analysis for a suite of simulation design. *Atmos. Res*. 169, 280–291.

MONIN, A.S.; OBUKHOV, A.M. 1954. Basic laws of turbulent mixing in the surface layer of the atmosphere. *Contrib Geophys Inst Acad Sci USSR* 24(151), 163–187.

MOONEY P.A.; MULLIGAN, F.J.; FEALY, R. 2011. Comparison of ERA-40, ERA-Interim and NCEP/NCAR reanalysis data with observed surface air temperatures over Ireland. *Int. J. Climatol*. 31(4), 545–557.

MOYA-ÁLVAREZ, A.S.; ESTEVAN, R.; KUMAR, S.; FLORES ROJAS, J.L.; TICSE, J.J.; MARTÍNEZ-CASTRO, D.; SILVA, Y. 2020. Influence of PBL parameterization schemes in WRF_ARW model on short - range precipitation's forecasts in the complex orography of Peruvian Central Andes. *Atmos. Res*. 233, 104708.

ONWUKWE, C.; JACKSON, P.L. 2020. Meteorological downscaling with wrf model, version 4.0, and comparative evaluation of planetary boundary layer schemes over a complex coastal airshed. *J. Appl. Meteorol. Climatol.* 59(8), 1295–1319.

PÉREZ-JORDÁN, G.; CASTRO-ALMAZÁN, J.A.; MUÑOZ-TUÑÓN, C.; CODINA, B.; VERNIN, J. 2015. Forecasting the precipitable water vapour content: validation for astronomical observatories using radiosoundings. *Mon. Not. R. Astron. Soc*. 452(2), 1992–2003.

POWERS, J. G.; KLEMP, J. B.; SKAMAROCK, W. C.; DAVIS, C. A.; DUDHIA, J.; GILL, D. O.; … DUDA, M. G. 2017. The Weather Research and Forecasting Model: Overview, System Efforts, and Future Directions. *Bull. Am. Meteorol. Soc*. 98(8), 1717–1737.

PRASAD, A.A.; SHERWOOD, S.C.; BROGNIEZ, H. 2020. Using Megha-Tropiques satellite data to constrain humidity in regional convective simulations: A northern Australian test case. *Q. J. R. Meteorol. Soc*. 1–21.

RAO, V. K.; MITRA, A. K.; SINGH, K. K.; BHARATHI, G.; RAMAKRISHNNA, S. S. V. S.; SATEESH, M.; … RAMESH, K. J. 2020. Validating INSAT-3D atmospheric temperature retrievals over india using radiosonde measurements and other satellite observations. *Meteorol. Atmos. Phys*. 132(4), 583–601.

ROSAS, J.; HOUBORG, R.; MCCABE, M.F. 2017. Sensitivity of Landsat 8 Surface Temperature Estimates to Atmospheric Profile Data: A Study Using MODTRAN in Dryland Irrigated Systems. *Remote Sens*. 9(10), 988.

RUIZ, J.J.; SAULO, C.; NOGUÉS-PAEGLE, J. 2010. WRF Model Sensitivity to Choice of Parameterization over South America: Validation against Surface Variables. *Mon. Weather Rev*. 138(8), 3342–3355.

SAHA, S.; MOORTHI, S.; WU, X.; WANG, J.; NADIGA, S.; TRIPP, P.; … BECKER, E. 2014. The NCEP Climate Forecast System Version 2. *J. Clim*. 27(6), 2185–2208.

SANTOS, D.C.; NASCIMENTO, E.D.L. 2016. Numerical Simulations of the South American Low Level Jet in Two Episodes of MCSs: Sensitivity to PBL and Convective Parameterization Schemes. *Adv. Meteorol*. 2016, 1–18.

SHERWOOD, S.C.; ROCA, R.; WECKWERTH, T.M.; ANDRONOVA, N.G. 2010. Tropospheric water vapor, convection, and climate. *Rev. Geophys*. 48(2), RG2001.

SKAMAROCK, W. C.; KLEMP, J. B.; DUDHIA, J.; GILL, D. O.; ZHIQUAN, L.; BERNER, J.; … HUANG, X.-Y. 2019. A Description of the Advanced Research WRF Model Version 4, *NCAR Technical Note* NCAR/TN-475+STR. Boulder, Colorado.

SOBRINO, J.A.; COLL, C.; CASELLES, V. 1991. Atmospheric correction for land surface temperature using NOAA-11 AVHRR channels 4 and 5. *Remote Sens. Environ*. 38(1), 19–34.

SOBRINO, J.A.; JIMÉNEZ-MUÑOZ, J.C.; MATTAR, C.; SÒRIA, G. 2015. Evaluation of Terra/MODIS atmospheric profiles product (MOD07) over the Iberian Peninsula: a comparison with radiosonde stations. *Int. J. Digit. Earth* 8(10), 771–783.

STENSRUD, D.J. 2007. *Parameterization Schemes, Parameterization Schemes: Keys to Understanding Numerical Weather Prediction Models*. Cambridge University Press, Cambridge.

STULL, R. 2017. *Practical Meteorology: An Algebra-based Survey of Atmospheric Science*, 1.02b. ed. University of British Columbia, Vancouver.

TARDY, B.; RIVALLAND, V.; HUC, M.; HAGOLLE, O.; MARCQ, S.; BOULET, G. 2016. A Software Tool for Atmospheric Correction and Surface Temperature Estimation of Landsat Infrared Thermal Data. *Remote Sens*. 8(9), 696.

THORNE, P.W.; PARKER, D.E.; CHRISTY, J.R.; MEARS, C.A. 2005. Uncertainties in climate trends: Lessons from upper-air temperature records. *Bull. Am. Meteorol. Soc*. 86(10), 1437–1442.

TONOOKA, H. 2001. An atmospheric correction algorithm for thermal infrared multispectral data over land-a water-vapor scaling method. *IEEE Trans. Geosci. Remote Sens*. 39(3), 682–692.

TYAGI, B.; MAGLIULO, V.; FINARDI, S.; GASBARRA, D.; CARLUCCI, P.; TOSCANO, P.; … GIOLI, B. 2018. Performance analysis of planetary boundary layer parameterization schemes in WRF modeling set up over Southern Italy. *Atmosphere*. 9(7), 1–22.

WANG, W.; BRUYERE, C.; MICHAEL, D.; DUHIA, J.; DAVE, G.; KAVULICH, M. … RIZVI, S. 2019. Advanced Research WRF (ARW) Version 4 Modeling System User´s Guide. National Center for Atmospheric Research. Retrieved from https://www2.mmm.ucar.edu/wrf/users/docs/user_guide_V4/WRFUsersGuide.pdf

WEE, T.K.; KUO, Y.H.; LEE, D. K.; LIU, Z.; WANG, W.; CHEN, S.Y. 2012. Two overlooked biases of the advanced research wrf (arw) model in geopotential height and temperature. *Mon. Weather Rev*. 140(12), 3907–3918.

XIE, B.; FUNG, J.C.H.; CHAN, A.; LAU, A. 2012. Evaluation of nonlocal and local planetary boundary layer schemes in the WRF model. J. Geophys. Res. Atmos. 117(12), 1–26.